Algal Research 49 (2020) 101907

Contents lists available at ScienceDirect

Algal Research

journal homepage: www.elsevier.com/locate/algal

Chlorella vulgaris heterotrophic colony development and interaction

Jing Zhang, Thi-Bich-Thuy Tran, Behnam Taidi, Pin Lu, Patrick Perré*

Université Paris-Saclay, CentraleSupélec, Laboratoire de Génie des Procédés et Matériaux, SFR Condorcet FR CNRS 3417, Centre Européen de Biotechnologie et de Bioéconomie (CEBB), 3 rue des Rouges Terres, 51110 Pomacle, France

ARTICLE INFO

Keywords:
Chlorella vulgaris
Heterotrophic growth
3D imagery
Colony growth model
Packing factor
Glucose consumption

ABSTRACT

This study is a first outcome of a series of works on immobilized cultures of *Chlorella vulgaris*. Colonies were grown independently on solid media under heterotrophic conditions and their growth was followed by continuous three-dimensional microscopy and image analysis. The growth was assessed by 3D imaging using a structured light microscope and subsequent image processing. Based on the expressions proposed for the height and radius growth dynamics, we concluded that the colonies expanded at a constant rate in the horizontal direction and a decreasing rate in the vertical direction. A spherical cap best describes the shape of the colonies during the growth period. During development, the packing density of the cells in the colony was calculated to occupy 25–40% of the available space. The cell yield was initially much lower than published values and approached those values at the end, indicating that the glucose consumption was dependent on not only the growth and division of cells but also on the activity of old cells. Finally, no colony-colony intraspecies interaction was observed when two colonies were grown in proximity.

1. Introduction

Chlorella vulgaris is a well-studied spherical microalga. This species is a potential candidate for commercial biofuel and food production due to its robustness, high growth rate, and lipid content [1]. An essential species in co-culture systems [2], *C. vulgaris* has four different cultivation modes: photoautotrophic, heterotrophic, mixotrophic, and photoheterotrophic [3–5]. Although photoautotrophic growth attracts much interest as CO_2 is fixed during the process, heterotrophic growth is also desirable because of the increased production of biomass and lipids, yet with cheaper and simpler bioreactor design and an easier scaling-up process [3,6].

A colony of microorganisms is a natural community grown on solid medium and exposed to the headspace gases, and is an easily detectable life form that responds to any change induced by the species [7], mutation [8], domestication [9], and some cultivation conditions. The last includes pH, temperature [10], agar concentration, nutrient concentrations [11], and the presence of other organisms that exert influence through numerous mechanisms such as quorum sensing molecules [12–14], physical contact [15], and nutrient competition [14,16]. To further investigate these phenomena, in the current study, the development of a single colony and colony-colony intraspecies interactions were studied.

The chlorophyll molecule of *C. vulgaris* is naturally fluorescent with a peak emission range of 680–690 nm [17], allowing easy observation of the colonies using at wide-field stereo fluorescence microscope equipped with structured illumination (Zeiss Axio Zoom. V16). This equipment enables high-resolution 3D images to be acquired rapidly and circumvents several disadvantages, such as the potential photobleaching of confocal laser scanning microscopy [18], destructive observation of living samples in electron microscopy [19], and the restriction induced by the rotating stage of micro three-dimension computed tomography [20].

Mathematical models have always been a complement and a consolidation for the study of biological experiments to understand, make predictions, or check hypotheses [21]. The traditional continuous population-based models play an important role in biological research due to their simplicity and computational efficiency [22]. A number of published empirical growth models have been used to simulate microbial growth under homogeneous conditions, notably, the Monod, Verhulst, Gompertz, and Richards equations and their variants [23]. Simple physical-biological models have also been developed to depict radial-growth and height-growth of colonies in a heterogeneous environment [24]. However, no unified colony growth model has been designed, especially for microalgae.

The purpose of this study was to investigate the colony development of *C. vulgaris* under heterotrophic conditions. The absence of light ensured that a single energy and carbon source exists during the growth,

* Corresponding author.
E-mail address: patrick.perre@centralesupelec.fr (P. Perré).

https://doi.org/10.1016/j.algal.2020.101907
Received 30 January 2020; Received in revised form 9 March 2020; Accepted 2 April 2020

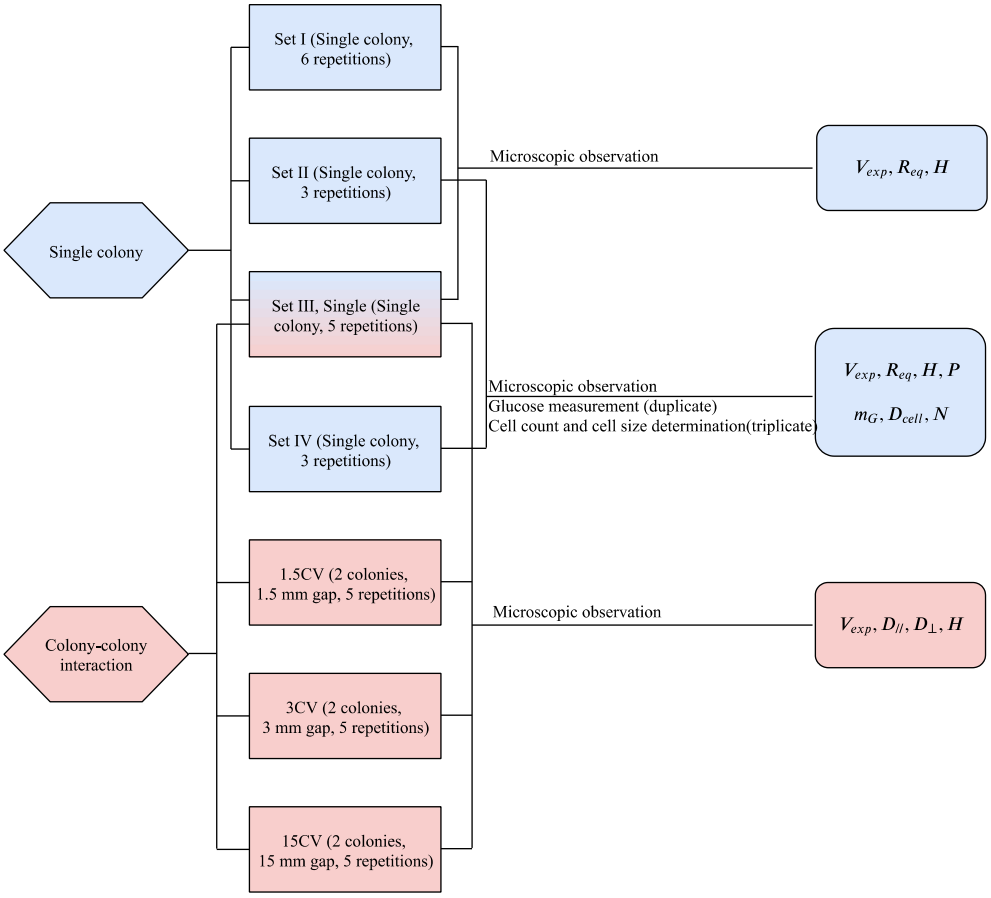

Fig. 1. Flow chart of experiment design. Hexagons represent the two series of experiments in the study, and rectangles represent the experiments. The phrases preceding the parentheses are the short names of the experiments (used hereafter in the text). In the parentheses, 'single colony' and '2 colonies' indicate the number of microcolonies inoculated in a Petri dish; '1.5 mm gap', '3 mm gap', and '15 mm gap' represent the initial distance between the two microcolonies. Experiment set III is designated as 'single' in the second topic. Rounded rectangles refer to the measured variables: V_{exp} is the measured volume, R_{eq} the equivalent radius, H the height, P the packing factor (defined as the volume fraction occupied by cells in the colony), m_G the mass of glucose in the medium at time t, D_{cell} the average diameter of cells, N the total number of cells, and $D_{//}$ and $D_{\perp}$ the parallel and orthogonal diameters of the colony, respectively.

whatever the position in the colony. It eased the result interpretation and allowed us to propose a simple and efficient interpretation of colony development. This first step was required before dealing with mixotrophic conditions (works in progress), for which the metabolic pathway depends on the position within the colony (organic carbon in the medium and carbon dioxide in air as carbon sources, and the former and presence of light on the top of the colony as energy sources, but with rapid attenuation in internal layers). First, a theoretical model was proposed, then a single colony growth experiment was performed to demonstrate the volume, radius, and height dynamics, and the model parameters were established by regression. The experiment also revealed the relationship between the cell population and the volume of the colony, and therefore, the volume fraction occupied by cells. This allowed the biomass growth to be continuously quantified. The cell yield was analyzed and compared with published values and finally, the spatial-temporal interaction between two neighboring colonies was investigated in terms of height, and parallel and orthogonal directions in the horizontal plane. Based on the series of observations and analysis method developed and validated in the current work, this reliable non-destructive 3D imaging method offered a tool the study of more complex situations in the future, e.g., colony growth under photo-autotrophic and mixotrophic conditions, interaction of species in the co-culture system (autotrophy and heterotroph). In addition, the proposed biological and numerical models laid a foundation to reveal the metabolism pathways of heterotrophic growth colony, which always exist, at least at the bottom part of the colony due to the absence of light.

2. Materials and methods

2.1. Strain and media

Chlorella vulgaris SAG 211-12 was obtained from the Culture Collection of Algae (SAG), University of Göttingen, Germany. To obtain the inoculum, this strain was grown in B3N liquid medium [25] (50 mL medium in 250 mL Erlenmeyer flask) at 25 °C, 170 rpm, with 1.0% (*v*/v) CO_2, under 30 μmol·m^{-2}·s^{-1} continuous LED illumination on the surface of the cultures in the microbial incubator (INFORS HT Minitron, Switzerland). A seven-day-old culture was selected for the inoculation of colonies.

Colonies were grown on MBM-GP solid medium [2]. It was composed of B3N medium in which the concentration of $NaNO_3$, $CaCl_2{\cdot}2H_2O$, $MgSO_4{\cdot}7H_2O$, and FeEDTA were doubled and combined with 20 g·L^{-1} of peptone, 20 g·L^{-1} of agar, and 10 g·L^{-1} of glucose (D(+)-Glucose, ≥ 99%, anhydrous, ACROS Organics™). The glucose solution was autoclaved separately to avoid caramelization. Approximately 15 mL MBM-GP medium at approximately 50 °C was poured into each Petri dish (50 mm diameter, pre-sterilized, THERMO FISHER, UK), and gelified at room temperature. A nitrocellulose membrane (0.2 μm pore, 47 mm diameter, Sartorius Stedim Biotech GmbH, Germany) was then placed on the surface of the solid medium before inoculation. The membrane was imprinted with a 3 mm × 3 mm grid, which was used as a scale and to guide the colony inoculation placement position.

2.2. Sampling procedures and growth conditions

To obtain the inoculum, a 15 mL pre-sterilized tube with 10 mL liquid culture was centrifuged for 5 mins at 4 °C at 8586 *g* (Centrifuge, 5804 R, Eppendorf, Germany). Then, approximately 9 mL of the

supernatant was discarded, and the remaining culture was transferred to a 1.5 mL sterilized tube. This tube was centrifuged again for 5 mins at 4 °C at 6800 g. After discarding the supernatant, a trace of cells was carefully inoculated onto the membrane with a sterilized 2.5 μL micro-tip. After inoculation, the Petri dishes were sealed by parafilm, covered with aluminum foil to prevent exposure to light, and incubated at 25 °C and 70% relative humidity in a dark incubator (Memmert HPP 400, Schwabach).

2.3. Experimental design

The following chart (Fig. 1) graphically outlines the experimental design.

Two series of experiments were performed (Fig. 1). In the 'single colony' series, there were four sets of experiments designed to observe the spatial-temporal development of a single colony in a Petri dish. In sets I and III experiments, a single colony was observed continuously for 666 h. In sets II and IV, the results were collected from different colonies that were destroyed at various times to determine the total number of cells and the glucose consumption rate during growth. These four independent experiment sets increased the reliability of the results.

The interaction between two colonies was studied by inoculating them in a Petri dish with an initial gap of 1.5 mm, 3 mm, or 15 mm. The 'colony-colony interaction' series were performed using the same protocol as set III, which served as control.

2.4. Image acquisition

3D fluorescent images of the colonies were obtained using the Zeiss Axio Zoom.V16 stereo fluorescence microscope (Carl Zeiss Microscopy GmbH, Germany) combined with Apotome2 and objective Apo Z 1.5×, a short-arc mercury reflector lamp (HXP200, ZEISS, Germany) at 75% light intensity, and a 63 HE filter set (BP 559–585 nm, BS 590 nm, BP 600–690 nm).

Stacks of images with a pixel size of 6.5 μm in the x-y-plane and 6.5 μm spacing in the z-axis were taken with a 50 ms exposure time per image. The software of ZEN 2.3 pro (blue edition, ZEISS, Germany) was used to control the microscope system. The image resolution was 512 × 512 pixels, which represents a field width of 3.33 mm × 3.33 mm. As the colony grew, several (multi-tile) images were required to cover the entire colony in the x-y-plane. At the end of one typical observation, 2 × 2 tiles are required to cover the total colony field. To limit the image acquisition time to 30 min per colony, the spacing in the z-axis was increased to 13 μm after 240 h of incubation.

2.5. Image analysis and measurement

The primary steps of image processing were devoted to 3D reconstruction. The out-of-focus information was first removed using a function of the ZEN 2.3 pro software and the native czi format (raw format of images produced by microscope) was converted to TIFF format, using either ZEN 2.3 Pro or ImageJ. For multi-tile images, the conversion was performed after stitching by ImageJ [26,27].

The images were further processed using an in-house code developed in Matlab® 2018b. The image processing operation included median filtering to reduce the noise, an automatic threshold based on the maximum entropy method and morphological operations on the binary image (filtering, endpoints connection, hole-filling, and closing). Then, the colony volume was built by merging all images of the stack. This allowed for growth parameters such as volume (V_{exp}), height (H), and equivalent radii (R_{eq}) to be determined automatically. The flowchart of the image processing chain is summarized in Fig. 2, and the post-processed binary 3D images of a single *C. vulgaris* colony from set III are represented for selected times in Fig. 3.

To compute the shape parameters, simple assumptions were made regarding the colony shape:

- The volume increment between two slices is assumed to be a truncated cone,
- The colony radius R_{eq} is determined from the maximum slice area, assuming that the colony-membrane interface is circular,
- The height H is the distance between the last visible slice of the stack and the first slice of images with an area greater than half the maximum area. Indeed, as the colony is not exactly parallel to the focus plane of the microscope, the plane with at least half the maximum area is considered the bottom of the colony.

Using these assumptions, the colony volume at time t is computed as follows:

$$V_{exp}(t) = \sum_{i=1}^{n-1} \left[\frac{1}{3} \times \Delta z \times (a_i + a_{i+1} + \sqrt{a_i \cdot a_{i+1}}) \right] \quad (1)$$

where i is the slice index, n the number of the non-empty slices, a_i the area of slice i, and Δz the distance between slices.

The equivalent radius $R_{eq}(t)$ is determined as:

$$R_{eq}(t) = \sqrt{\frac{max\{a_1,\ldots,a_n\}}{\pi}} \quad (2)$$

where $max\{a_1,\ldots,a_n\}$ is the maximum area of all slices, which is the best representative of the area of the colony at the membrane level.

For the 'colony-colony interaction' experiments, the two diameters in the parallel directions degenerate into one single transect after colony merging. In this case, the equivalent radius can no longer be defined. Thus, the sum of $D_{//}$ of the two colonies is used as an indicator before merging, and the total length $D_{//}$ is used after merging (Fig. 4). The diameter in the orthogonal direction $D_{\perp}$ represents the average value of the two colonies before and after merging (Fig. 4).

2.6. Cell enumeration and packing factor

The population of a colony was estimated by suspending the entire colony in water and determining the cell concentration in the suspension using a Beckman Coulter counter (Multisizer™ 4 COULTER COUNTER®, California, United States). The total cell number was obtained by the determined concentration multiplied by the total suspension volume. The average diameter of cells was also obtained with the Coulter counter. Each measurement was performed in triplicate.

Once the colony was photographed through the microscope, a 12 mm × 12 mm square membrane containing the whole colony was cut by a disposable pre-sterilized scalpel, added to a 15 mL tube containing 400 μL fresh Milli-Q (BioPak®) water, and the tube vortexed to a homogeneous suspension. The suspension was diluted to an OD 800 nm between 0.2 and 0.4, and average cell diameter and total cell concentration were determined by the Coulter counter equipped with a 30 μm diameter aperture.

For the series of tests using destructive measurement at selected times, the cell number and the average cell size of the colony was determined by the Coulter counter. These data allowed for the calculation of the total volume occupied by cells. The packing factor $P(t)$ of cells in a colony is defined as the total cell volume (assuming the cell to be spherical) divided by the colony volume:

$$P(t) = 4\pi/3 \times \left(\frac{D_{cell}(t)}{2} \right)^3 \times N(t)/V_{exp}(t) \quad (3)$$

where $D_{cell}(t)$ is the average cell diameter, $N(t)$ the total number of cells, and $V_{exp}(t)$ the apparent volume of the colony determined by image processing.

2.7. Dry matter content

Five 168-hour-old colonies were collected to determine the dry matter content. These five colonies were transferred to a 50 mL tube

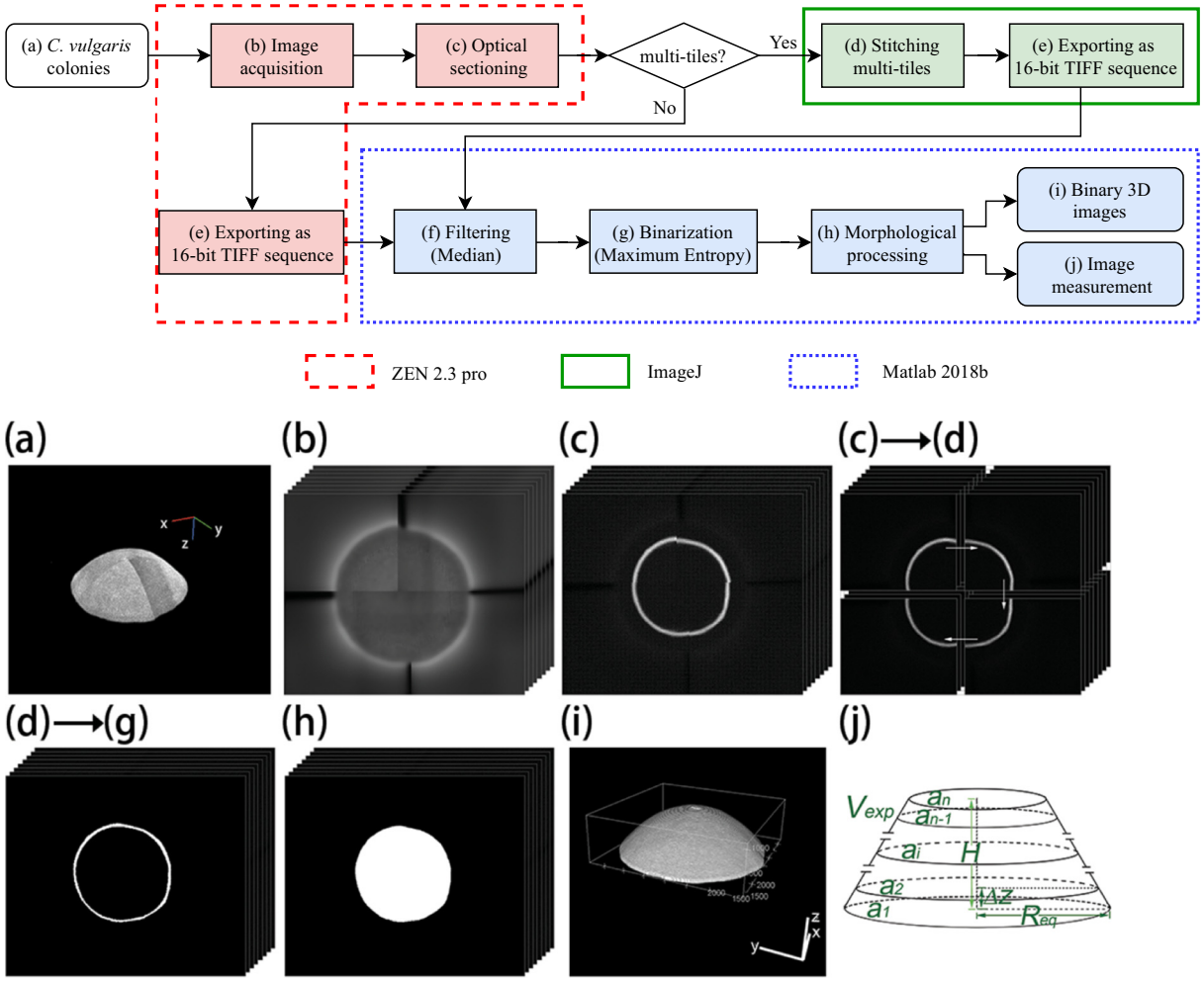

Fig. 2. Flow chart of image processing and measurement. (a) The *C. vulgaris* colony, microscopic version. (b) The acquired images by Zeiss Axio Zoom.V16 (e.g., a stack of 4 tiles and 8 slices images). (c) The optical sectioning of the images obtained by ZEN 2.3 pro. (d) The post-stitching images in which the four tiles have been merged into one. (c)➔(d) shows the theory of the stitching based on the stitching plugin of ImageJ [26,27]. (e) The native czi format images are converted to TIFF format and saved as a sequence by ImageJ or ZEN 2.3 pro. (f) The denoised sequence obtained using the median filter. (g) The binarized sequence with a threshold value calculated by the maximum entropy algorithm [28,29]. (h) The sequence obtained by a series of morphological processing steps, such as filtering, thinning, endpoints connection [30], filling, dilation, and erosion. (i) Reconstruction and measurement of the colony. The schematic diagram shows the measurement theory for the equivalent radius (R_{eq}), the area of the colony at the *i*-th slice (a_i), the distance between neighbor slices (Δz), and the height of the colony (H). The volume of the colony (V_{exp}) is the sum of the parts between slices, which is measured under the assumption that each part is a circular truncated cone.

with 5000 µL fresh Milli-Q water to obtain a suspension (as in Section 2.6). Then, 100 µL of this suspension was used to determine the cell concentration and the cell size using the Beckman Coulter counter. To determine the dry mass, the remaining 4900 µL was centrifuged for 10 min at 2 °C at 4950 g, and then the pellet was washed and centrifuged twice again with the same conditions. The final pellet was transferred to a pre-weighed aluminum dish (pre-dried to constant weight at 105 °C) and then dried to a constant weight at 105 °C. Each measurement was performed in triplicate. The following equation was used to calculate dry matter content R_{dry} (the ratio of dry mass over wet mass):

$$R_{dry} = \frac{m_{tot} - m_{tare}}{N \times \rho_{wet} \times 4\pi/3 \times (D_{cell}/2)^3} \quad (4)$$

where m_{tot} is the total mass (aluminum dish and pellet) after dehydration, m_{tare} the mass of the aluminum dish, N total number of cells, D_{cell} the average cell diameter and ρ_{wet} the cell density set at 1.11 g·mL^{-1} (the cell density of 7-day-old *Chlorella* sp. from [31]).

2.8. Glucose measurements

The glucose concentration was measured using high-performance liquid chromatography (HPLC, Ultimate 3000, Thermo Scientific, USA) with a cationic column (Aminex HPX−87H, 300 mm × 78 mm, Bio-Rad, USA). The nitrocellulose membrane with its colony attached was removed from the Petri dish, and the dish with the remaining medium was then weighed (m_M). The solid medium was diluted with 25× its weight in Milli-Q water, heated to 97 °C with continuous stirring (200 rpm), then cooled to 25 °C using an ice water bath, resulting in a melted growth medium solution. The solution was filtered using a 0.2 µm membrane (PP Syringe, Whatman™ Puradisc™, VWR International, France) and 10 µL of this filtrate was analyzed by HPLC (at 60 °C with a flow rate of 0.5 mL·min^{-1} using isocratic elution with 2 mM H_2SO_4 as a mobile phase). The refractive index (RI) detector (RI 101, Shodex, Japan) was fixed at 35 °C to obtain signal values. The calibration curve of glucose was obtained by 5-point external calibration in the range of 0.2 g·L^{-1} − 10 g·L^{-1} D (+)-Glucose (≥99%, anhydrous, ACROS Organics™, Czech Rep). The total run time of each injection was 30 min. The glucose concentration, $c(t)$, was quantified as the peak area. In order to obtain the right glucose balance, the

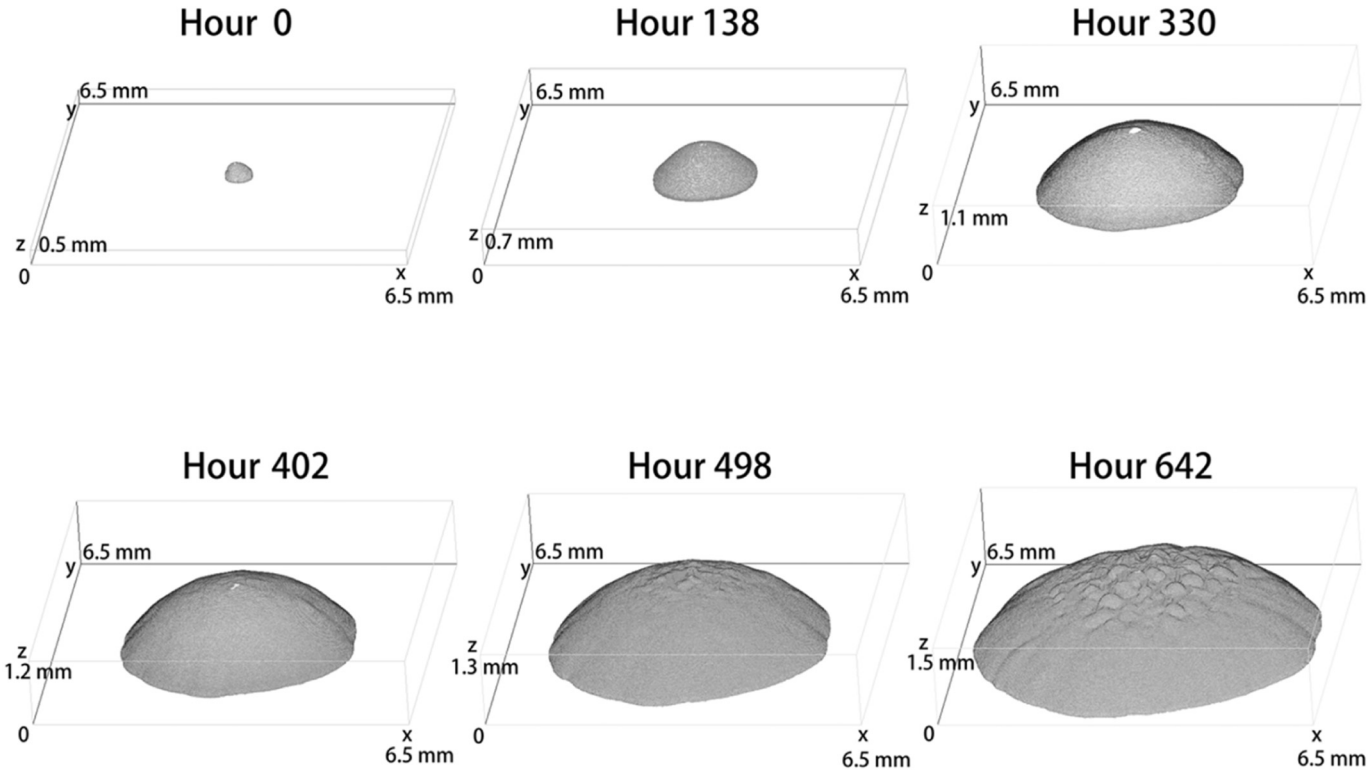

Fig. 3. Post-processed 3D images of a single *C. vulgaris* colony from set III.

evolution of medium mass should be taken into account:

$$m_G(t) = c(t) \times (m_M(t) - m_P) \quad (5)$$

where m_P is the mass of empty Petri dish, $m_M(t)$ the mass of Petri dish with the solid medium at time t, $m_G(t)$ the mass of glucose at time t, and $c(t)$ the glucose concentration at time t.

3. Results and discussion

3.1. Biological model of single colony development

To understand the mechanism of colony development, colonies were cut in the middle by a scalpel (Fig. 5a) and the cross-sections of the colonies were then observed by Zeiss Axio Zoom.V16. Two differently-aged colonies were observed at the margin (M), top (T), and bottom (B) segments independently, and the center (C) of the 336-hour-old colony was also observed (Figs. 5b and 5c). Those cells in the center of the 336-hour-old colony were densely arranged and most of them had ruptured and lost their cell integrity while they were intact in other colony locations.

Following these observations, a simple mechanism of colony development can be proposed. For the young colony (Fig. 5b), most cells were alive with a complete structure and no apparent differences in cell morphology were observed. It is reasonable to postulate that the cells at the outer boundary of the colony (margin cells) divide for the radial growth of the colony, as these cells benefit from an exposure to unlimited nutrients [32] and from a stable supply in O_2 likely to penetrate the colony at that location due to its small height [33–35]. The cells in the middle of the colony near the membrane benefit from unlimited nutrients but might suffer from a lack of O_2 needed to diffuse from the top of the colony. Those top cells maintain a complete structure but with decreased activity due to limited nutrients needed to diffuse across

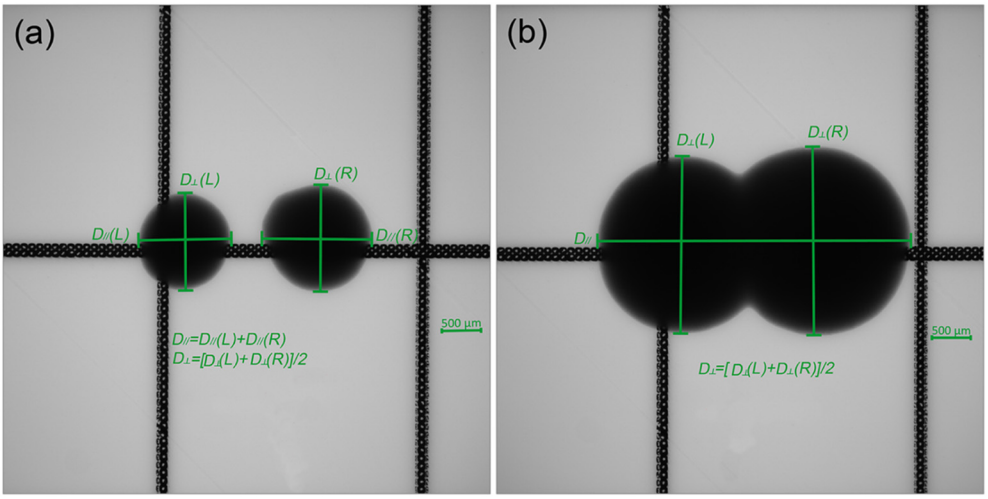

Fig. 4. Demonstration of adjacent colony diameter measurements in the parallel ($D_{//}$) and orthogonal directions ($D_\perp$). (a) Measurement of $D_{//}$ and $D_\perp$ before merging. $D_{//}$ is the sum of the two colonies in the parallel direction, $D_\perp$ is the average value of the two colonies in the orthogonal direction. (b) Measurement of $D_{//}$ and $D_\perp$ after merging. $D_{//}$ is the total length of the merged colony. $D_\perp$ is the same as that of before merging. Scale bar, 500 μm.

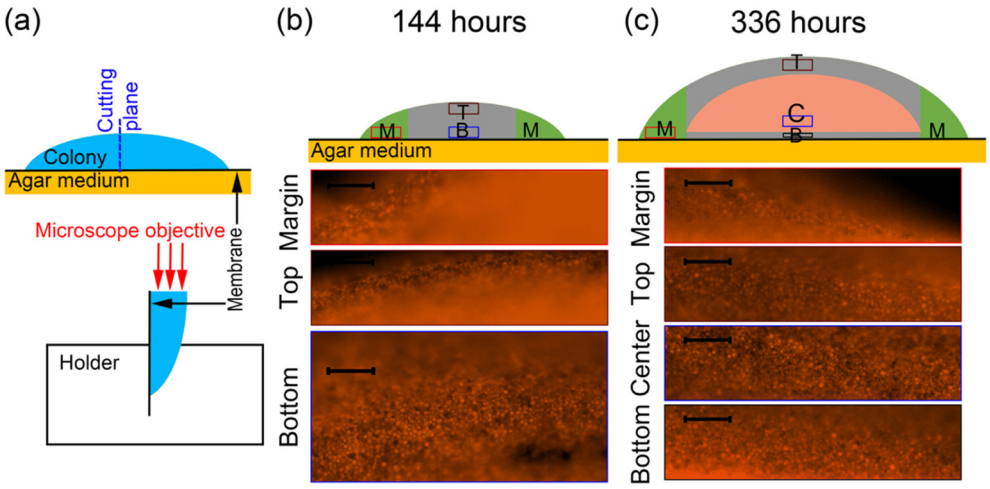

Fig. 5. Single colony development analysis. (a) Schematic diagram of the experiment. The colony was cut by a scalpel in the middle and the physical cross-section was turned towards the microscope objective. Then, the cross-sections of 144-h-old and 336-h-old colonies were photographed, shown in (b) and (c), respectively. The observed shapes of colonies are shown in the drawings (b) and (c) with an indication of different zones: M (Margin, in green), T (Top, in gray), B (Bottom, in gray), and C (Center, in red). Scale bar, 50 μm. (For interpretation of the references to colour in this figure legend, the reader is referred to the web version of this article.)

the colony.

In the old colony (Fig. 5c), the cells at the margin and the top functioned similarly to the related cells in the young colony. A center segment developed where the cells lose their structure (Fig. 5c). Those center cells suffer a lack of both nutrients and oxygen. They undergo autopathy to supply nutrients for the survival and division of top cells [36]. For the top colonies, the nutrients might be derived from both the autopathic cells and the medium. A decreasing growth of the colony with increasing height would occur as the nutrients become more limited due to increasing distance from the medium. The cells at the very bottom layers may have divided because of the abundant nutrient supply and, likely, some O_2 diffuses through the medium.

3.2. Numerical model of single colony development

3.2.1. Radial growth

According to the above observations, we postulate that an external layer of cells at the margin of the colonies, Δr ensures radial growth. This layer undergoes the same growth conditions regardless of the age of the colonies [37]. The extension rate of colonies in the radial direction should, therefore, be constant, and the following expression could determine the evolution of radius over time:

$$R_{eq}(t) = R_{eq}(t_0) + \mu_{max}\Delta r t \tag{6}$$

where t is the age of the colony, $R_{eq}(t_0)$ and $R_{eq}(t)$ the equivalent radii of the colony at times t_0 and t, respectively, μ_{max} the maximum specific growth rate of *C. vulgaris* cell (a constant value of 0.05 h^{-1} from the suspension culture, unshown data), and Δr the growth width at the margin of the colony. A linear model measured R_{eq} using expression (6). Note that this procedure allows only the product $\mu_{max}\Delta r$ to be identified. The obtained value of Δr therefore depends on the value used for μ_{max}.

3.2.2. Vertical growth

Following the observation and assumptions of Section 3.1 for the vertical development, we postulate that change in height over time should demonstrate asymptotic behavior due to the increased nutrient limitation with height. The following expression was chosen for the time evolution of height (t):

$$H(t) = H_{max}\left[1 - e^{\left(-\frac{t-t_{H0}}{\tau_H}\right)}\right] \tag{7}$$

where t is the age of the colony, H_{max} the maximum possible height, t_{H0} the time shift needed to get the initial height of the inoculum at $t = 0$, and τ_H the time constant of height growth.

3.2.3. Shape characteristics of colonies

The volume of the colony depends not only on the height and equivalent radius but also on its shape. To describe the shape characteristics of a colony in a simple and measurable way, a variable called shape ratio was used, which is defined as the ratio between the volume of a standard pattern and the real volume of the colony. In our study, cylinder and spherical cap were the two considered standard patterns, and the corresponding shape ratios could be calculated as follows:

(i) For a cylindrical pattern, the shape ratio $\eta_c(t)$ is defined as

$$\eta_c(t) = V_{exp}(t)/V_c(t) \tag{8}$$

where $V_c(t)$ is the volume of the cylinder at time t:

$$V_c(t) = \pi R_{eq}(t)^2 H(t) \tag{9}$$

(ii) For a spherical cap pattern, the shape ratio $\eta_s(t)$ is defined as

$$\eta_s(t) = V_{exp}(t)/V_s(t) \tag{10}$$

where $V_s(t)$ is the volume of the spherical cap at time t:

$$V_s(t) = \frac{1}{6}\pi H(t)[3R_{eq}(t)^2 + H(t)^2] \tag{11}$$

To define a unique shape ratio $\eta(t)$, the two candidate shape ratios $\eta_c(t)$ and $\eta_s(t)$ were compared. Then, we determined $\eta(t)$ with the selected shape ratio as a function of time:

$$\eta(t) = \eta_{st}/\left[1 - e^{\left(-\frac{t-t_{\eta 0}}{\tau_\eta}\right)}\right] \tag{12}$$

where t is the age of the colony, η_{st} the asymptotic stable shape ratio of the colony, $t_{\eta 0}$ the time shift necessary for the initial inoculation shape, and τ_η the time constant of the change in colony shape.

3.3. Colony growth

Four independent sets of experiments were performed to study the development of single *C. vulgaris* colonies. The experiment sets II and IV were destructive. For each time point, triplicate colonies were measured by 3D imaging and then destroyed for glucose determination. The total number of cells and the average diameter of cells were also determined using the Coulter counter.

As expected, colony radii expanded linearly and expansion was constant during the entire experiment. This is demonstrated by the excellent fit obtained using expression (6) ($Adj\text{-}R^2 > 0.99$, Table. 1 and Fig. 6a). Assuming the maximum growth rate of *C. vulgaris* to be 0.05 h^{-1}, and an average cell diameter of 4 μm, the circumferential growth zone (Δr) was approximately 67–89 μm, equivalent to 17–22

Table 1
Summary of all parameters fitted from the experimental results using the proposed growth models.

Experiment	Experiment data				Fit*										
	Initial value				$R_{eq}(t)$			$H(t)$				$\eta(t)$			
	V_{exp}	R_{eq}	H	Ratio R_{eq}/H	$R_{eq}{}^*(t_0)$	Δr	$Adj\text{-}R^2$	$\tau_H{}^*$	$t_{H0}{}^*$	H^*_{max}	$Adj\text{-}R^2$	$\tau_\eta{}^*$	$t_{\eta 0}{}^*$	$\eta_{st}{}^*$	$Adj\text{-}R^2$
	μm	μm	μm		μm	μm		h	h	μm		h	h		
Set I	4.4×10^7	336	141	2.38	262	74	0.998	700	−30	2318	0.993	118	−105	0.98	0.973
Set II	3.9×10^7	322	142	2.27	275	67	0.991	726	−35	2229	0.996	110	−100	0.99	0.866
Set III	3.6×10^7	264	234	1.13	313	89	0.997	354	−43	1616	0.997	74	−150	0.98	0.736
Set IV	5.5×10^7	367	150	2.45	422	68	0.995	636	−45	2026	0.993	86	−96	1.11	0.962

Note: values marked with (*) indicate that they are from the fit with Eqs. (6), (7), and (12).

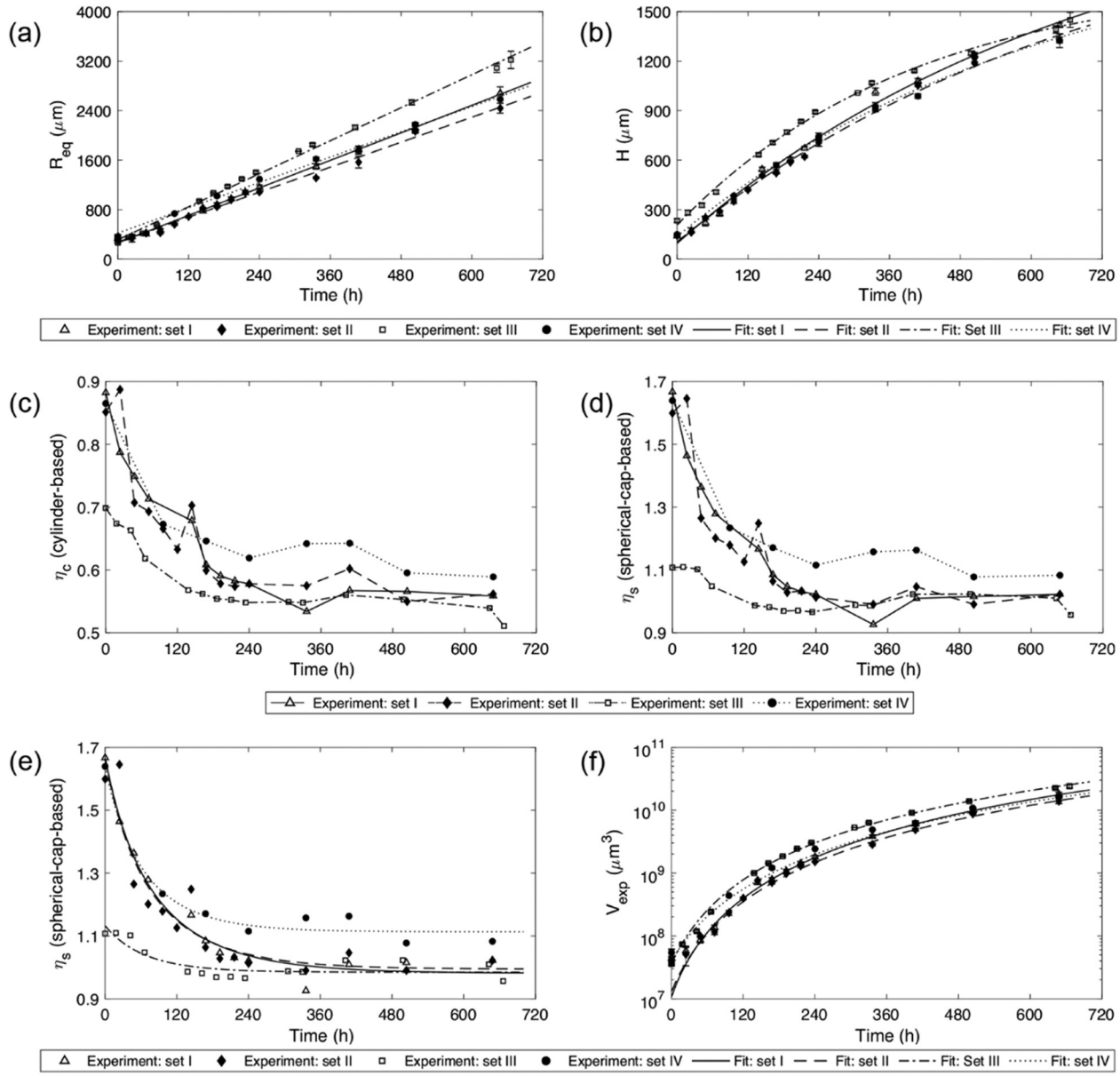

Fig. 6. *Chlorella vulgaris* colony development. (a) Colony development in the horizontal direction. (b) Colony development in the vertical direction. Graphs (c) and (d) show the shape ratios of the colony based on the cylinder and spherical cap, respectively. (e) The fit of the selected shape ratio (spherical-cap-based). (f) The volume of colonies. The experiment sets I, II, III, and IV are represented by empty triangles, filled diamonds, empty squares, and filled circles, respectively. In graphs (a), (b), (e), and (f), the predicted equivalent radii, heights, shape ratios, and volume calculated by Eqs. (6), (7), (12), and (11) are represented by the solid line, dashed line, dotted line, and dash-dotted line, respectively. Error bars represent standard error.

layers of cells at the outer boundary of the colony.

As postulated in Section 3.1, a decreasing growth rate was observed in height. The experimental height from all four sets fit Eq. 7 well ($Adj\text{-}R^2 > 0.99$, Table 1 and Fig. 6b). The maximum height of colonies was calculated as (sets 1–4, respectively) 2318 μm, 2229 μm, 1616 μm, and 2026 μm, suggesting that the maximum height of *C. vulgaris* colonies was approximately 2 mm under these specific experimental conditions.

An alternative way to model the growth of colonies is to consider them as regular patterns. The two models of the cylinder and spherical cap were compared with the actual volume measurements (Fig. 6c and d), and the shape ratio was defined at the same time (see Section 3.2.3). The spherical-cap-based shape ratio proved to be more stable over the culture and provided the best approximation. This observation suggests that the colony shape remained globally spherical and kept its spherical cap form over time (Fig. 6e). Thus, the spherical-cap-based shape ratio was selected as a unique shape ratio in this work. This result is in agreement with the 3D reconstructed views, as depicted in Supplementary Figs. S1 and S2.

Altogether, the colony development in the horizontal direction, vertical direction, and pattern could be predicted by the equivalent radius model (Eq. (6)), height model (Eq. (7)), and shape ratio model (Eq. (12)), respectively. Consistently, the volume of the colony could be predicted as a function of time by a combination of these models, with good agreement with the experimental volume (Fig. 6f).

3.4. Cell-level analysis

In experimental sets II and IV, the colonies were first observed to obtain their volumes and subsequently treated to obtain the number of cells in the colony and their average size using Coulter counter.

The colony volume and the number of cells present in the colony both exhibited a gradually decreasing slope in the semi-log curve (Figs. 7a and b), and they demonstrated an excellent global correlation with each other (Fig. 7c). An excellent linear fit was obtained in log-log scale: $\ln N(t) = 0.86 \ln V_{exp}(t) + 7.04$ ($Adj\text{-}R^2 = 0.98$), where $N(t)$ is the number of cells and $V_{exp}(t)$ the colony volume at time t. Previous researchers have reported direct relationships between the number of cells and the area of colonies [38], the relationship between area and the visible cell numbers of the colony [38,39], and the relationship between the radius of the colony and the visible cell numbers [40]. In the present study, the correlation was more consistent as it considered the influence of the whole colony volume instead of merely its area.

In spite of the relationship between the number of cells and the colony volume, cell size change over time in the colony exhibits significant variation (Fig. 7d). The average diameter initially increased from 3.3 μm to 4.6 μm during the first 144 h, and then gradually decreased to its initial diameter at the end of the experiment (Fig. 8). This behavior is consistent with that reported for *Escherichia coli* [41].

To investigate further the spatial distribution of cells, the packing factor change over time was determined using Eq. (3). The packing factor represented only 15% of the total volume just after inoculation and gradually increased during culture growth to 30% at 96 h. It stabilized near this value up to the end of the culturing period. With an average cell diameter of 4 μm, the volume of the cell equals 33.5 μm^3, which gives a density of 10^{17} cell·m^{-3}, consistent with the value reported in a recent study [42].

3.5. Glucose consumption

The glucose consumption may be derived as the product of glucose mass needed per dry mass of microalgae (inverse of cell yield Y_{cell} in the mass of dry cell per mass of glucose) times the mass of microalgae produced $m_{cell}(t)$:

$$\frac{dG}{dt} = 1/Y_{cell}\frac{dm_{cell}}{dt} \tag{13}$$

The production of dry mass of cells can be expressed as the wet volume of cells, assuming their wet density ρ_{wet} to be equal to 1.11 g·mL^{-1} times the dry mass content R_{dry}:

$$\frac{dG}{dt} = \rho_{wet}\frac{R_{dry}}{Y_{cell}}\frac{d(V_{wet})}{dt}$$

The glucose consumption, therefore, depended on both the variation of cell number $N_{cell}(t)$ and the variation of the average cell size $D_{cell}(t)$, as determined with the Coulter counter. Assuming the cells to be spherical, we obtain

$$\frac{dG}{dt} = \rho_{wet}\frac{R_{dry}}{Y_{cell}}\left[4\pi/3 \times (D_{cell}(t)/2)^3 \times \frac{d(N_{cell})}{dt} + N_{cell}(t) \times 4\pi/3 \times \frac{d((D_{cell}(t)/2)^3)}{dt}\right] \tag{14}$$

From our culture, the average dry matter content, R_{dry}, determined using the protocol explained in Section 2.7 (Eq. (4)) was 66%. Note that up to 91% percent of intercellular water could be included in the microorganism pellet (which traditionally has been used to determine the cell wet mass), which would give a dry mass content result of 57% [43]. In addition, our method is consistent with the method used to compute the volume of wet cells in Eq. (14).

In our experiments, all measurements were of samples taken from the culture at discrete times t_i. Assuming all new cells formed were the size measured at t_{i+1}, the respective contributions of cell division and cell size variation to the change of dry mass over the time interval $[t_i, t_{i+1}]$ would be

$$\left(\frac{dm_{dry}}{dt}\right)_{division} = \rho_{wet}\, R_{dry}\, 4\pi/3 \times ((D_{cell})_{i+1}/2)^3 \times (N_{i+1} - N_i)$$

$$\left(\frac{dm_{dry}}{dt}\right)_{size} = \rho_{wet}\, R_{dry}\, N_i \times 4\pi/3 \times (((D_{cell})_{i+1}/2)^3 - ((D_{cell})_i/2)^3)$$

Both contributions are depicted in Fig. 9. In experiment set II, the variation rate of total dry mass due to the variation in cell size decreased from 7.8×10^{-8} g·h^{-1} to -5.8×10^{-7} g·h^{-1}, while that due to cell division increased from 5.5×10^{-8} g·h^{-1} to 9.1×10^{-6} g·h^{-1}. Set IV yielded similar results: the variation rate of total dry mass on cell size decreased from 4.2×10^{-8} g·h^{-1} to -1.8×10^{-6}g·h^{-1}, while that on cell division increased from 7.1×10^{-7} g·h^{-1} to 1.1×10^{-5} g·h^{-1}. Comparing the absolute values, the change in total dry mass of cells after the initial sampling was mostly due to cell division.

From Eq. (13) and experimental values (shown in Fig. 9), the cell yield (Y_{cell}) during culture time can be determined (Table 2). The yield using the total variation of dry mass and yield obtained by neglecting the change of cell size confirmed that glucose demand was primarily controlled by cell division. At the beginning of the immobilized cultures (namely, up to ca. 400 h), our experimental values of Y_{cell} were much lower than values reported previously (Table 2). It is reasonable to presume that during initial colony growth, the enormous glucose consumption is used not only for those new cells to grow and divide but also for old cells to remain metabolically active [44]. Moreover, it might be because fermentation yields less energy than *C. vulgaris* respiration [45]. During later growth, the cell yield became more stable and was closer to the range of published values. This is likely due to cells growing less active or dying and glucose consumption being directed to cell division, which is consistent with the proposed biological model (Section 3.1), where active cells concentrate on the edge of the colonies.

3.6. Colony-colony interaction

To study the interaction between two *C. vulgaris* colonies, the

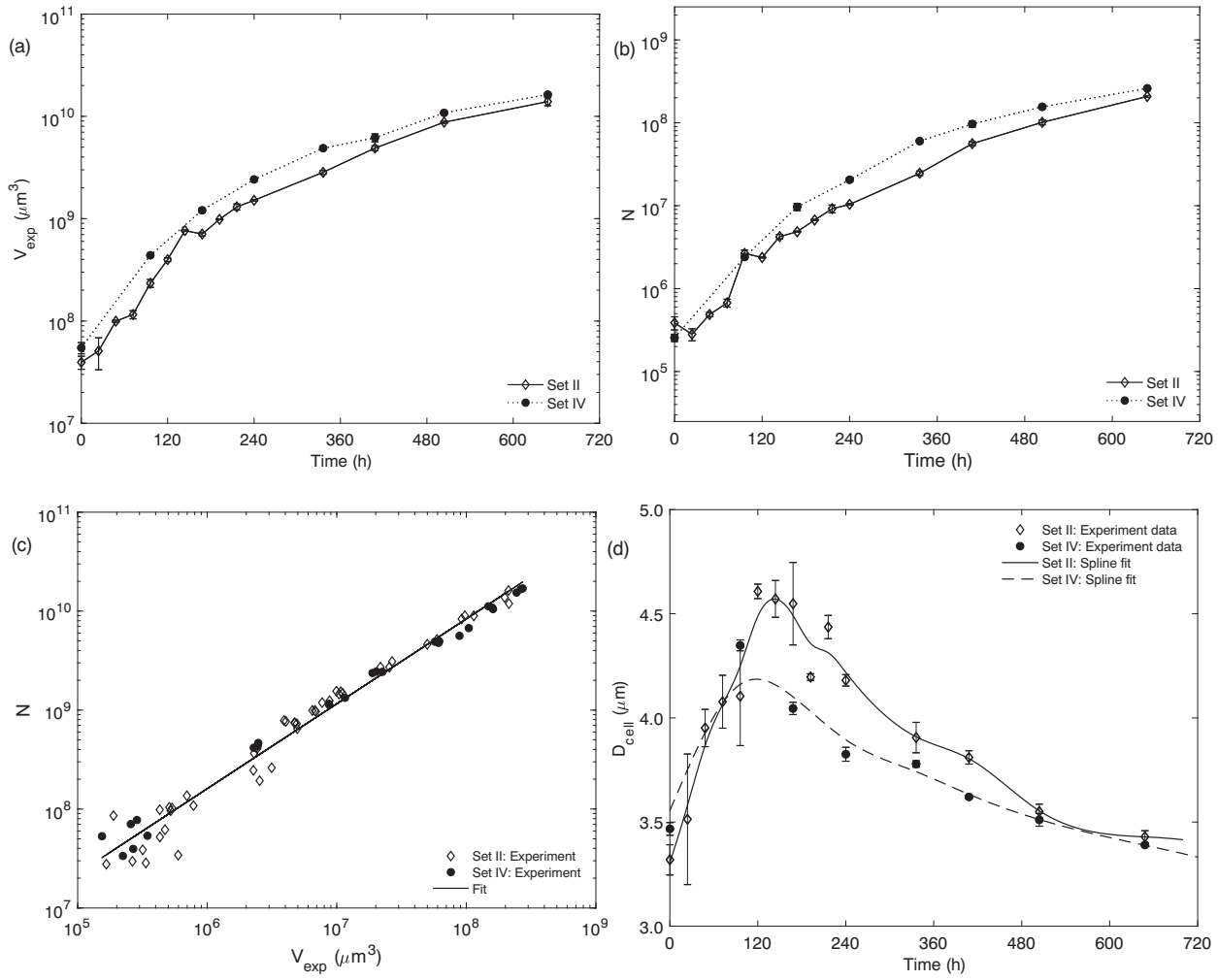

Fig. 7. (a) Volume growth. (b) Population growth. (c) The relationship between natural logarithm (ln) of the volume and the number of cells. (d) The average diameter of cells. Empty diamonds and filled circles represent the data of experiment sets II and set IV, respectively. The solid and dashed lines are the splines fit of sets II and set IV, respectively. Error bars represent standard error.

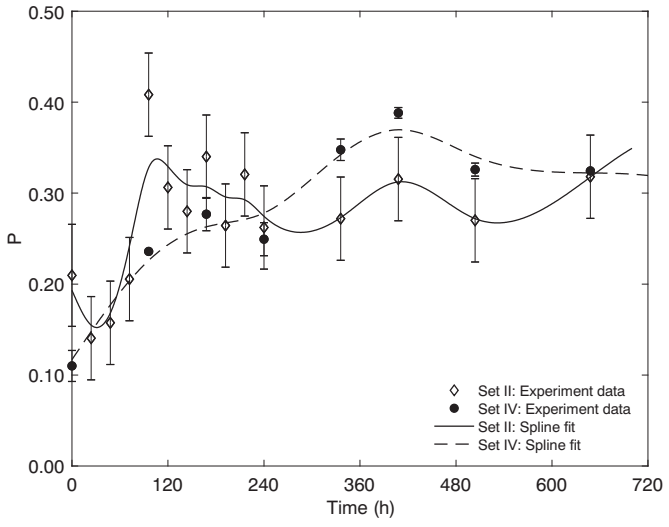

Fig. 8. Packing factor of the colony. The packing factor *P* is the occupied ratio of cells in the colony. Empty diamonds and filled circles represent the data of experiment sets II and IV, respectively. The solid and dashed lines are the splines fit of sets II and IV, respectively. Error bars represent standard error.

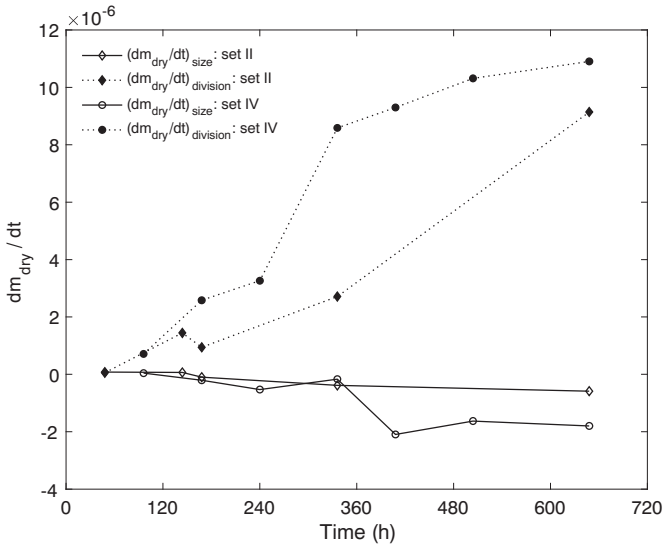

Fig. 9. Changes in total dry mass of cells for experimental sets II and IV. One can observe that the change in total dry mass of cells was mostly due to cell division after initial sampling.

Table 2
Experimental cell yield.

Experiment	Time Hour	Cell yield (Y_{cell}) g dry cell/g glucose	
		Accounting for change in cell size	Neglecting change in cell size
Set II	48	0.004	0.002
	144	0.026	0.025
	168	0.022	0.025
	336	0.654	0.762
	648	0.295	0.315
Set IV	96	0.008	0.007
	168	0.040	0.044
	240	0.124	0.148
	336	0.204	0.208
	408	0.337	0.435
	504	0.513	0.609
	648	0.228	0.273
References	[46]	0.457–0.475[a]	
	[47]	0.539–0.694	
	[48,49]	0.787[b]	

[a] Is adapted from the value of 82.4–85.6 g cell/mol glucose from reference [46].

[b] Is adapted from the cited references: value of 83% C of glucose +1% C of cellular producing 72% C of cellular from reference [48]; and value of 43.46% Carbon/cellular from reference [49].

colonies were incubated under four different conditions: single colony as a control (single), two colonies with an initial distance of 1.5 mm (1.5CV), two colonies with an initial distance of 3 mm (3CV), and two colonies with an initial separation distance of 15 mm (15CV). Five replicate plates were set up for each experiment and the average results are shown with their standard errors. The two 1.5CV colonies merged at 138 h, the 3CV colonies at 306 h and no merging occurred during the experiment for the 15CV colonies (Supplementary Fig. S3). Similar to the 'single colony' experiments, the 'colony-colony interaction' experiments were analyzed in terms of horizontal growth, vertical expansion, and volume development. However, to follow the colonies before and after merging, we used the parallel and orthogonal diameters $D_{//}$ and $D_{\perp}$ (see Section 2.5) instead of R_{eq} from the 'single colony' experiment.

The heights of all the four experiments were fitted with Eq. (7) ($Adj\text{-}R^2 > 0.99$, Fig. 10a and Table 3). All the double colonies had a maximum height of about 2 mm which was the same as in the single colony experiments. The diameter evolution was also fitted using Eq. (6) before the colony merging (Table 3). The double width (the diameter is analyzed here instead of the radius) of the growth layer was approximately 180 μm (Fig. 10b), which is in agreement with the value used for the single colony experiments. The $D_{//}$ growth of the single and the 15CV colonies remained linearly throughout the experimental period, while the 1.5CV and 3CV colonies showed two linear growth phases (Fig. 10c). After merging, the slope was divided by a factor of two. This is consistent with the definition of $D_{//}$, which accounts for four dividing fronts before merging and only two after merging. This observation does not depend on the initial distance between the colonies; it only changes the merging time. The factor half in the slope indicates that the growth rate at the outside part of the margin was not affected by the merging.

Similarly, in the case of 15CV, where the colonies did not merge at all, there was no significant influence of the presence of another *C. vulgaris* colony on diametral growth.

The total volume of the colonies (the sum of the two colony volumes) grew at a decreasing rate (Fig. 10d), which was also similar to the 'single colony' experiments. All colonies experienced a similar growth rate before 138 h. After merging at 138 h, the 1.5CV colonies grew more slowly than the other colonies. This is easily explained by the fact that the total length of the dividing margin was reduced after merging, which limited the increase of total surface area over time.

In conclusion, all these observations indicate that a *C. vulgaris* colony is not influenced by the presence of another colony of the same

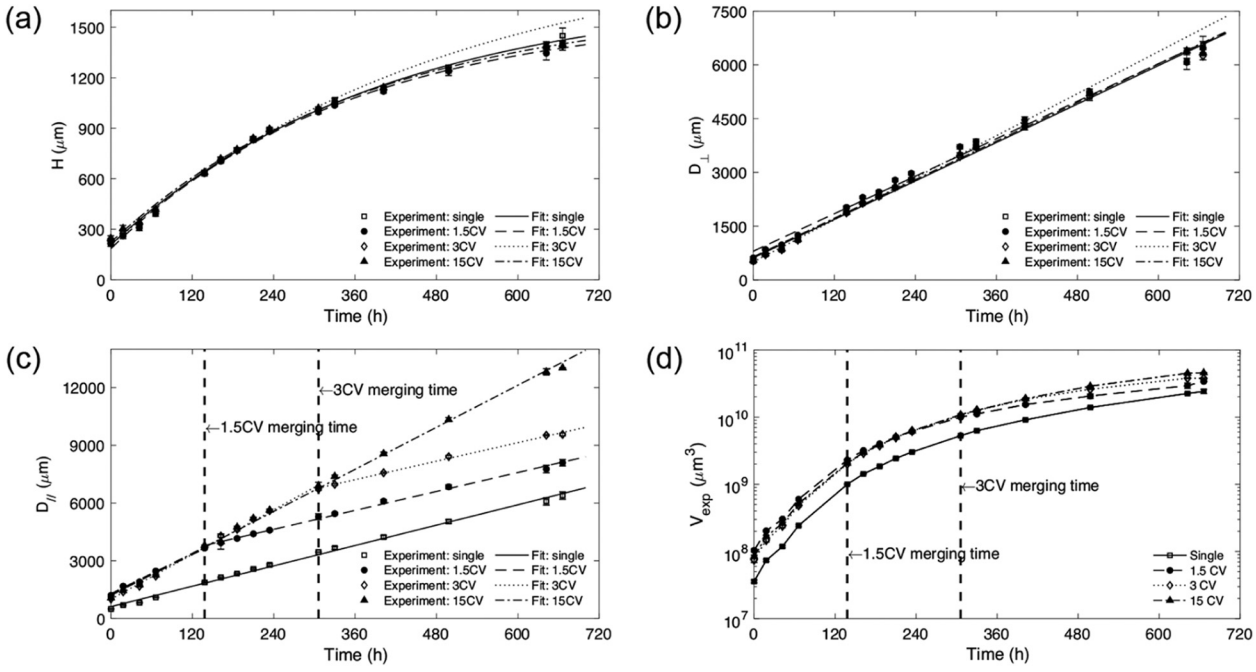

Fig. 10. Colony-colony interaction of *C. vulgaris*. (a) Development of height *H*. Graphs (b) and (c) are colony development in the orthogonal direction ($D_{\perp}$) and parallel direction ($D_{//}$), respectively (see Section 2.5). (d) Volume growth. Single colony (single), two colonies with the initial distance of 1.5 mm (1.5CV), 3 mm (3CV) and 15 mm (15CV) are represented by empty squares, filled circles, empty diamonds, and filled triangles, respectively. In graphs (a), (b) and (c), the predicted *H*, $D_{\perp}$, and $D_{//}$ of the single, 1.5CV, 3CV, and 15CV were obtained by Eqs. (7), (6), and (6), and they are represented by solid line, dashed line, dotted line, and dash-dotted line, respectively. In graph (c), the value of $D_{//}$ of experiments 1.5CV and 3CV was fitted using Eq. (6) by two different sets of parameters before and after merging. Error bars represent standard error.

Table 3
Fitness of the diameter of colonies under different inoculation conditions.

Conditions		Experimental data			Fit*									
		Initial value			H				$D_{\perp}$			$D_{//}$		
		H	$D_{\perp}$	$D_{//}$	$\tau_H{}^*$	$t_{H0}{}^*$	H^*_{max}	$Adj\text{-}R^2$	$D^*_{\perp}(t_0)$	$\Delta D_{\perp}$	$Adj\text{-}R^2$	$D^*_{//}(t_0)$	$\Delta D_{//}$	$Adj\text{-}R^2$
		µm	µm	µm	h	h	µm		µm	µm		µm	µm	
Single		234	518	500	401	−52	1709	0.997	615	179	0.996	622	176	0.996
1.5CV	Before merging	215	614	1203	492	−54	1984	0.995	801	174	0.991	1263	349	0.991
	After merging											2668	164	0.995
3CV	Before merging	228	525	1015	382	−55	1650	0.998	503	196	0.998	1011	387	0.996
	After merging											4511	150	0.988
15CV		246	550	1062	356	−44	1593	0.997	644	179	0.996	1201	364	0.988

Note: values marked with (*) indicate that they are from the fit with Eqs. (6) and (7).

strain in the neighborhood. In particular, the growth in height and the radial growth at the external margin of the colony were not affected. The reduction in total volume growth is explained simply by a geometrical effect: the total length of external margin, responsible for the area extension, was just reduced after merging.

4. Conclusion

In this work, we focused on the growth of one isolated and two adjacent *C. vulgaris* colonies. Based on the proposed biological growth model, which takes into account the impact of oxygen and nutrients, two mathematical models, a linear radial and an asymptotic height growth, were developed, and their consistency tested experimentally. Additionally, a spherical cap was the shape that best described the quantitative and morphological growth of the colony. No interaction was observed between two *C. vulgaris* colonies growing at an initial distance of 1.5 mm, 3 mm, and 15 mm. In particular, no effect on height growth and radial growth was detected even after colony merging that occurred in the colonies initially separated by 1.5 mm and 3 mm. The decrease in volume growth observed after merging was explained simply by the reduction of the external margin, where division occurred. Thanks to this validated method of immobilized cultures and related analysis protocol, works are in progress in our team to study the metabolism pathways of colonies under heterotrophic and mixotrophic conditions. To that purpose, we designed culture support able to measure gas concentrations continuously. Furthermore, the proposed numerical models and features of colonies could be used to investigate interspecies interaction in co-culture system (e.g., quorum sensing).

Statement of informed consent

No conflicts, informed consent, human or animal rights applicable. The authors agree to the submission of the manuscript for peer review and publication in *Algal Research*.

CRediT authorship contribution statement

Jing Zhang: Conceptualization, Methodology, Investigation, Formal analysis, Writing - original draft. **Thi-Bich-Thuy Tran**: Methodology, Writing - review & editing. **Behnam Taidi**: Conceptualization, Methodology, Writing - review & editing. **Pin Lu**: Methodology, Writing - review & editing. **Patrick Perré**: Conceptualization, Methodology, Formal analysis, Writing - review & editing.

Acknowledgments

This study was carried out in the Centre Européen de Biotechnologie et de Bioéconomie (CEBB), supported by Région Grand Est, Département de la Marne, Grand Reims and the European Union. In particular, the authors would like to thank Département de la Marne for its financial support. The authors thank Cédric Guerin of LGPM for the help in HPLC glucose analysis.

Declaration of competing interest

The authors declare that they have no known competing financial interests or personal relationships that could have appeared to influence the work reported in this paper.

Appendices. Appendix A. Supplementary Figs. S1 and S2; Appendix B. Supplementary Fig. S3

Supplementary data to this article can be found online at https://doi.org/10.1016/j.algal.2020.101907.

References

[1] C. Sa, B. Zebib, O. Merah, P.Y. Pontalier, C. Vaca-Garcia, Morphology, composition, production, processing and applications of *Chlorella vulgaris*: a review, Renew. Sust. Energ. Rev. 35 (2014) 265–278, https://doi.org/10.1016/j.rser.2014.04.007.
[2] A. La, P. Perré, B. Taidi, Process for symbiotic culture of *Saccharomyces cerevisiae* and *Chlorella vulgaris* for in situ CO_2 mitigation, Appl. Microbiol. Biotechnol. 103 (2019) 731–745, https://doi.org/10.1007/s00253-018-9506-3.
[3] O. Perez-garcia, Y. Bashan, Microalgal heterotrophic and mixotrophic culturing for bio-refining: From metabolic routes to techno-economics, Algal Biorefineries, Springer, 2015, pp. 61–131, , https://doi.org/10.1007/978-3-319-20200-6.
[4] K.L. Yeh, J.S. Chang, Effects of cultivation conditions and media composition on cell growth and lipid productivity of indigenous microalga *Chlorella vulgaris* ESP-31, Bioresour. Technol. 105 (2012) 120–127, https://doi.org/10.1016/j.biortech.2011.11.103.
[5] T.M. Mata, A.A. Martins, N.S. Caetano, Microalgae for biodiesel production and other applications: a review, Renew. Sust. Energ. Rev. 14 (2010) 217–232, https://doi.org/10.1016/j.rser.2009.07.020.
[6] J. Hu, D. Nagarajan, Q. Zhang, J.S. Chang, D.J. Lee, Heterotrophic cultivation of microalgae for pigment production: a review, Biotechnol. Adv. 36 (2018) 54–67, https://doi.org/10.1016/j.biotechadv.2017.09.009.
[7] A. Suchwalko, I. Buzalewicz, A. Wieliczko, H. Podbielska, Bacteria species identification by the statistical analysis of bacterial colonies Fresnel patterns, Opt. Express 21 (2013) 11322–11337, https://doi.org/10.1364/oe.21.011322.
[8] C. Di Franco, E. Beccari, T. Santini, G. Pisaneschi, G. Tecce, Colony shape as a genetic trait in the pattern-forming *Bacillus mycoides*, BMC Microbiol. 2 (2002) 1–15, https://doi.org/10.1186/1471-2180-2-33.
[9] V. Šťovíček, L. Váchová, M. Begany, D. Wilkinson, Z. Palková, Global changes in gene expression associated with phenotypic switching of wild yeast, BMC Genomics 15 (2014) 136, https://doi.org/10.1186/1471-2164-15-136.
[10] A. Draeger, S. Wray, E.B. Babiychuk, Domain architecture of the smooth-muscle plasma membrane: regulation by annexins, Biochem. J. 387 (2005) 309–314, https://doi.org/10.1042/BJ20041363.
[11] S. Tasaki, M. Nakayama, W. Shoji, Morphologies of *Bacillus subtilis* communities responding to environmental variation, Develop. Growth Differ. 59 (2017) 369–378, https://doi.org/10.1111/dgd.12383.
[12] A. Be'er, H.P. Zhang, E.-L. Florin, S.M. Payne, E. Ben-Jacob, H.L. Swinney, Deadly competition between sibling bacterial colonies, Proc. Natl. Acad. Sci. 106 (2009) 428–433, https://doi.org/10.1073/pnas.0811816106.
[13] Z. Palková, B. Janderová, J. Gabriel, B. Zikánová, M. Pospísek, J. Forstová, Ammonia mediates communication between yeast colonies, Nature 390 (1997)

532–536, https://doi.org/10.1038/37398.
[14] R. Paul, T. Ghosh, T. Tang, A. Kumar, Rivalry in *Bacillus subtilis* colonies: enemy or family? Soft Matter 15 (2019) 5400–5411, https://doi.org/10.1039/c9sm00794f.
[15] L.S. van Overbeek, K. Saikkonen, Impact of bacterial-fungal interactions on the colonization of the endosphere, Trends Plant Sci. 21 (2016) 230–242, https://doi.org/10.1016/j.tplants.2016.01.003.
[16] P. Frey-Klett, P. Burlinson, A. Deveau, M. Barret, M. Tarkka, A. Sarniguet, Bacterial-fungal interactions: hyphens between agricultural, clinical, environmental, and food microbiologists, Microbiol. Mol. Biol. Rev. 75 (2011) 583–609, https://doi.org/10.1128/mmbr.00020-11.
[17] T. Teplicky, M. Danisova, M. Valica, D. Chorvat, A. Marcek Chorvatova, Fluorescence properties of *Chlorella* sp, Algae, Adv. Electr. Electron. Eng. 15 (2017) 352–357, https://doi.org/10.15598/aeee.v15i2.2015.
[18] R.S. Fischer, Y. Wu, P. Kanchanawong, H. Shroff, C.M. Waterman, Microscopy in 3D: a biologist's toolbox, Trends Cell Biol. 21 (2011) 682–691, https://doi.org/10.1016/j.tcb.2011.09.008.
[19] M. Das Murtey, P. Ramasamy, Sample preparations for scanning electron microscopy–life sciences, Mod. Electron Microsc. Phys. Life Sci., IntechOpen (2016) 161–185, https://doi.org/10.5772/61720.
[20] D.W. Holdsworth, M.M. Thornton, Micro-CT in small animal and specimen imaging, Trends Biotechnol. 20 (2002) 34–39, https://doi.org/10.1016/S0167-7799(02)02004-8.
[21] F.L. Hellweger, R.J. Clegg, J.R. Clark, C.M. Plugge, J.U. Kreft, Advancing microbial sciences by individual-based modelling, Nat. Rev. Microbiol. 14 (2016) 461–471, https://doi.org/10.1038/nrmicro.2016.62.
[22] F.L. Hellweger, V. Bucci, A bunch of tiny individuals—individual-based modeling for microbes, Ecol. Model. 220 (2009) 8–22, https://doi.org/10.1016/j.ecolmodel.2008.09.004.
[23] M.H. Zwietering, I. Jongenburger, F.M. Rombouts, K. Van't Riet, Modeling of the bacterial growth curve, Appl. Environ. Microbiol. 56 (1990) 1875–1881, https://doi.org/10.1111/j.1472-765X.2008.02537.x.
[24] L.Z. Pipe, M.J. Grimson, Spatial-temporal modelling of bacterial colony growth on solid media, Mol. BioSyst. 4 (2008) 190–198, https://doi.org/10.1039/b708241j.
[25] B. Clément-Larosière, F. Lopes, A. Gonçalves, B. Taidi, M. Benedetti, M. Minier, D. Pareau, Carbon dioxide biofixation by *Chlorella vulgaris* at different CO2 concentrations and light intensities, Eng. Life Sci. 14 (2014) 509–519, https://doi.org/10.1002/elsc.201200212.
[26] M.D. Abràmoff, P.J. Magalhães, S.J. Ram, Image processing with ImageJ, Biophoton. Int. 11 (2004) 36–42.
[27] S. Preibisch, S. Saalfeld, P. Tomancak, Globally optimal stitching of tiled 3D microscopic image acquisitions, Bioinformatics 25 (2009) 1463–1465, https://doi.org/10.1093/bioinformatics/btp184.
[28] J.N. Kapur, Maximum-Entropy Models in Science and Engineering, John Wiley & Sons, 1989.
[29] F. Gargouri, Thresholding the Maximum Entropy, MATLAB Cent. File Exch. (2012) https://www.mathworks.com/ matlabcentral/fileexcha.
[30] C. Georges, Connect Two Pixels, MATLAB Cent. File Exch. (2004) https://www.mathworks.com/matlabcentral/ fileexcha.
[31] É.G. Baroni, K.Y. Yap, P.A. Webley, P.J. Scales, G.J.O. Martin, The effect of nitrogen depletion on the cell size, shape, density and gravitational settling of *Nannochloropsis salina*, *Chlorella* sp. (marine) and *Haematococcus pluvialis*, Algal Res. 39 (2019) 101454, , https://doi.org/10.1016/j.algal.2019.101454.
[32] J.A. Cole, L. Kohler, J. Hedhli, Z. Luthey-Schulten, Spatially-resolved metabolic cooperativity within dense bacterial colonies, BMC Syst. Biol. 9 (2015) 1–17, https://doi.org/10.1186/s12918-015-0155-1.
[33] A.C. Peters, J.W.T. Wimpenny, J.P. Coombs, Oxygen profiles in, and in the agar beneath, colonies of *Bacillus cereus*, *Staphylococcus albus* and *Escherichia coli*, Microbiology 133 (2009) 1257–1263, https://doi.org/10.1099/00221287-133-5-1257.
[34] L.E.P. Dietrich, C. Okegbe, A. Price-Whelan, H. Sakhtah, R.C. Hunter, D.K. Newmana, Bacterial community morphogenesis is intimately linked to the intracellular redox state, J. Bacteriol. 195 (2013) 1371–1380, https://doi.org/10.1128/JB.02273-12.
[35] S.P. Fraleigh, H.R. Bungay, Modelling of nutrient gradients in a bacterial colony, J. Gen. Microbiol. 132 (1986) 2057–2060, https://doi.org/10.1099/00221287-132-7-2057.
[36] L. Váchová, Z. Palková, How structured yeast multicellular communities live, age and die? FEMS Yeast Res. 18 (2018) 10000, , https://doi.org/10.1093/femsyr/foy033.
[37] P.T. Su, C.T. Liao, J.R. Roan, S.H. Wang, A. Chiou, W.J. Syu, Bacterial colony from two-dimensional division to three-dimensional development, PLoS One 7 (2012), https://doi.org/10.1371/journal.pone.0048098.
[38] E.-M. Rivas, E.G. de Prado, P. Wrent, M.-I. de Silóniz, P. Barreiro, E.C. Correa, F. Conejero, A.P. Murciano, J. M, A simple mathematical model that describes the growth of the area and the number of total and viable cells in yeast colonies, Lett. Appl. Microbiol. (2014), https://doi.org/10.1111/lam.12314.
[39] P.N. Skandamis, T.F. Brocklehurst, E.Z. Panagou, G.J.E. Nychas, Image analysis as a mean to model growth of *Escherichia coli* O157:H7 in gel cassettes, J. Appl. Microbiol. 103 (2007) 937–947, https://doi.org/10.1111/j.1365-2672.2007.03358.x.
[40] W.A. Harrison, A.C. Peters, L.M. Fielding, Growth of *Listeria monocytogenes* and *Yersinia enterocolitica* colonies under modified atmospheres at 4 and 8 degrees C using a model food system, J. Appl. Microbiol. 88 (2000) 38–43, https://doi.org/10.1046/j.1365-2672.2000.00848.x.
[41] H.J. Jeong, J. Kim, B.R. Levin, X. Shao, A. Mugler, I. Nemenman, Growth of bacteria in 3-d colonies, PLoS Comput. Biol. 13 (2017) e1005679, , https://doi.org/10.1371/journal.pcbi.1005679.
[42] P.K. Malakar, D.E. Martens, W. Van Breukelen, R.M. Boom, M.H. Zwietering, K. Van Riet, Modeling the interactions of *Lactobacillus curvatus* colonies in solid medium: consequences for food quality and safety, Appl. Environ. Microbiol. 68 (2002) 3432–3441, https://doi.org/10.1128/AEM.68.7.3432.
[43] G. Bratbak, I. Dundas, Bacterial dry matter content and biomass estimations, Appl. Environ. Microbiol. 48 (1984) 755–757.
[44] O. Perez-Garcia, L.E. de-Bashan, J.P. Hernandez, Y. Bashan, Efficiency of growth and nutrient uptake from wastewater by heterotrophic, autotrophic, and mixotrophic cultivation of *Chlorella vulgaris* immobilized with *Azospirillum brasilense*, J. Phycol. 46 (2010) 800–812, https://doi.org/10.1111/j.1529-8817.2010.00862.x.
[45] P.J. Syrett, H.A. Wong, The fermentation of glucose by *Chlorella vulgaris*, Biochem. J. 89 (1963) 308–315, https://doi.org/10.1042/bj0890308.
[46] T. Ogawa, S. Aiba, Bioenergetic analysis of mixotrophic growth in *Chlorella vulgaris* and *Scenedesmus acutus*, Biotechnol. Bioeng. 23 (1981) 1121–1132, https://doi.org/10.1002/bit.260230519.
[47] J. Doucha, K. Lívanský, Production of high-density *Chlorella* culture grown in fermenters, J. Appl. Phycol. 24 (2012) 35–43, https://doi.org/10.1007/s10811-010-9643-2.
[48] R.E. Burrell, C.I. Mayfield, W.E. Inniss, A carbon budget for heterotrophically grown *Ankistrodesmus braunii* and *Chlorella vulgaris*, MIRCEN J. Appl. Microbiol. Biotechnol. (1985), https://doi.org/10.1007/BF01742319.
[49] C.G. Khoo, M.H. Woo, N. Yury, M.K. Lam, K.T. Lee, Dual role of *Chlorella vulgaris* in wastewater treatment for biodiesel production: growth optimization and nutrients removal study, J. Japan Inst. Energy. 96 (2017) 290–299, https://doi.org/10.3775/jie.96.290.